Computers in Biology and Medicine 197 (2025) 110980

Contents lists available at ScienceDirect

Computers in Biology and Medicine

journal homepage: www.elsevier.com/locate/compbiomed

Beyond the neuron: Unveiling the role of reactive astrocytes in epileptic seizure dynamics through self-organized bistability

Yuliya Tsybina [a,b], Innokentiy Kastalskiy [b,c,*], Victor B. Kazantsev [a,b], Alexander E. Hramov [b,d,e], Susanna Gordleeva [a,b,d]

[a] Neuromorphic Computing Center, Neimark University, 6 Nartov St., Nizhny Novgorod, 603081, Russia
[b] Department of Neurotechnology, Lobachevsky State University of Nizhny Novgorod, 23 Gagarin Ave., Nizhny Novgorod, 603022, Russia
[c] Laboratory of Neurobiomorphic Technology, Moscow Institute of Physics and Technology, 9 Institutskiy Ln., Dolgoprudny, Moscow Region, 141701, Russia
[d] Baltic Center for Neurotechnology and Artificial Intelligence, Immanuel Kant Baltic Federal University, 14 Alexander Nevsky St., Kaliningrad, 236041, Russia
[e] Research Institute of Applied Artificial Intelligence and Digital Solutions, Plekhanov Russian University of Economics, 36 Stremyannyy Ln., Moscow, 115093, Russia

ARTICLE INFO

Keywords:
Spiking neural network
Reactive astrocyte
Neuron-astrocyte interaction
Extreme synchronization
Epileptiform activity

ABSTRACT

During epileptic seizures, brain activity and connectivity undergo dramatic changes. Brain networks transition from a balanced resting state to a hyperactive and hypersynchronous state. However, the mechanisms driving these state transitions remain unclear. While astrocyte-neuron interactions are increasingly recognized in seizure pathophysiology, fundamental questions about the causal role of astrocytes in seizure initiation and termination remain unanswered. To understand the dynamic network mechanisms of epileptic seizure initiation and propagation in interacting neural and astrocytic networks, we developed a biologically relevant spiking neural network model that incorporates reactive astrocytes. This model implements the transition from normal to epileptiform activity, including its spontaneous termination, without requiring manual parameter tuning or external stimulation. Using extensive numerical simulations, we demonstrate that the interplay between fast neuronal dynamics and the slower astrocyte-induced dynamic rearrangement of the neural network's functional architecture results in critical system behavior known as self-organized bistability. This self-organized dynamic regime is characterized by the spontaneous triggering of short-lived extreme synchronization events—a hallmark of epileptic seizure activity. The model generates trains of seizures, reproducing the distribution of intervals between seizures observed in neurophysiological experiments. We also show that gap junction connectivity within the astrocyte network plays a protective role against epileptic discharges. Collectively, our findings establish a unified framework where astrocyte-mediated self-organized bistability governs epileptiform dynamics, revealing glial networks as critical modulators of both seizure generation and suppression in pathological neural circuits.

1. Introduction

Epilepsy is a neurological disorder characterized by seizures, sudden, uncontrolled bursts of excessive or hypersynchronous neuronal activity in the brain [1]. These seizures can manifest in a variety of ways, depending on the specific brain regions involved. While epilepsy affects approximately 1% of the population, a significant portion (30%) remain unresponsive to traditional drug therapies [2–4]. Anti-seizure medications primarily act on neurons, providing symptom management but failing to alter the onset or progression of epilepsy. Moreover, they often carry serious adverse effects. This underscores the critical need for novel medications with distinct cellular and molecular targets and mechanisms of action.

To develop effective new therapies for epilepsy, we need to understand how seizures develop across different scales, from individual neurons to entire brain networks. Current epilepsy research has primarily focused on understanding how to suppress hypersynchronous neuronal activity that leads to seizures and on identifying the underlying changes in neuronal function or network activity that trigger these events [5]. This research focus has led to the widely accepted hypothesis that epileptic seizures arise from an imbalance between excitatory and inhibitory signaling within the brain [6–8]. This imbalance can result from a variety of factors, including changes in neurotransmitter levels, mutations in neurotransmitter receptors, ion

* Corresponding author.
E-mail address: kastalskiy@neuro.nnov.ru (I. Kastalskiy).

https://doi.org/10.1016/j.compbiomed.2025.110980
Received 1 June 2025; Received in revised form 11 August 2025; Accepted 18 August 2025

channels, and ion transporters, as well as alterations in the connections between neurons [9].

Although the study of the pathophysiology of epilepsy has revealed a variety of potential mechanisms of seizures initiation and propagation, the organization of neural networks and the mechanisms, which initiate profound changes in neural activity and connectivity observed during seizure is heavily debated [5,10,11].

Recently emerging evidence has also suggested a critical role for astrocytes in epilepsy [9,12,13], based on their multifaceted roles in buffering extracellular ions, clearing extra-cellular neurotransmitters, releasing gliotransmitters, and their production of inflammatory mediators [14–16]. Epilepsy triggers a shift in astrocytes' physiological state, known as "reactive astrogliosis", where these cells become "activated". This activation involves a complex and dynamic response to various pathological conditions. It encompasses a wide spectrum of changes, including genetic, epigenetic, molecular, metabolic, structural, and functional alterations. These changes are highly specific to the context and are regulated by specific signaling events. Reactive astrogliosis is a hallmark feature of the epileptic focus in both human patients and experimental models of epilepsy [13,15]. The exact role of interactions between reactive astrocytes and neurons in triggering and spreading epileptic seizures is still not fully understood, despite its potential for developing new therapies [17,18].

The communication between neurons and astrocytes operates on a slower timescale, spanning seconds to minutes, compared to the milliseconds-long timescale of neuronal firing and rapid synaptic transmission [19,20]. This difference in timing suggests that astrocyte-neuron communication serves distinct functions, potentially influencing synaptic strength, long-term synaptic plasticity, and the synchronization of neuronal activity within networks [21–23]. Astrocytes interact with neurons across multiple scales, from the nano- and microscales, influencing individual or multiple synapses within an astrocyte's territory, to syncytium-scale networks of astrocytes, connected through dynamic gap-junctions, that coordinate the excitability of functional neuronal ensembles and support their energetic demands, to coordinating activity across brain regions at the mesoscale [24].

Such complex organization of bidirectional interaction between astrocytic and neuronal networks is likely to produce multiscale spatiotemporal collective dynamics in both normal and pathological conditions. Considering that epilepsy is widely considered to be a phenomenon of a fundamentally nonlinear dynamic nature [5,25,26], complex network theory and biologically-realistic dynamical modeling offer powerful tools for exploring how different intrinsic and network properties can result in pathological activity, providing valuable insights for both clinicians and researchers.

At present, only a few models partially reproduce certain features of the disease at varying levels of detail, while considering the influence of astrocytes. Most mathematical modeling studies of epilepsy development in neuron-astrocytic ensembles investigate the influence of astrocytes on neuronal hyperexcitability in a biologically plausible and detailed manner, primarily at the cellular level [27–31]. Although hyperexcitability of individual neurons can significantly contribute to epileptogenesis, epilepsy is widely considered a "network disease" driven by aberrant synaptic interactions between neurons [5,32]. The importance of considering epilepsy at the network level is supported by experimental evidence linking alterations in astrocytic gap junction coupling with epilepsy in both rodents and human patients [33]. Few mathematical models explore the initiation and propagation of epileptic seizures in neuron-astrocytic networks [34–41]. Based on extensive experimental data on glutamate — the most intensively studied neuro- and gliotransmitter in epilepsy — some of these models investigate seizure-like discharges caused by abnormal glutamate uptake in astrocytes [34,35], while others describe how Ca^{2+}-dependent astrocytic glutamate release promotes neuronal synchronization [36–41]. These models depict epileptogenesis as a process in which a recurrent excitatory feedback loop is maintained through bidirectional signaling between neurons and astrocytes, leading to hypersynchronous neuronal activity. However, there is evidence that reactive astrocytes can release not only excitatory, but also inhibitory gliotransmitters in epilepsy, such as GABA. Studies have shown that despite the loss of GABAergic interneurons and synaptic inhibition in both human and experimental temporal lobe epilepsy, several studies have found that tonic (extrasynaptic) GABAergic currents remain normal or even increase. This suggests that elevated GABA levels are present, originating from sources outside of neurons [42–44]. Research indicates that reactive astrocytes might be the source of this extra GABA. These astrocytes may abnormally produce GABA through either new synthesis or the conversion of excess glutamate. This newly synthesized GABA is then released into the extracellular space, potentially via Best1 channels, where it activates tonic GABA receptors on excitatory neurons. This activation seems to counterbalance the loss of interneuron-mediated inhibition, reducing seizure susceptibility and potentially compensating for the compromised inhibitory system [43,44]. Moreover, experimental works show a protective function of the astrocytic network, preventing overexcitation and the spreading of neural activity epileptic bursts [17,45].

To summarize the above, existing computational approaches to epilepsy face several critical limitations:

1. Neuron-centric focus. Most models emphasize neuronal mechanisms while oversimplifying or ignoring glial contributions. This is particularly problematic given astrocytes' roles in regulating extracellular ions, neurotransmitters, and network excitability.
2. Scale limitations. While cellular-level models capture neuronal hyperexcitability, they often fail to address epilepsy as a network phenomenon. The emergent properties of neuron-astrocyte networks remain poorly understood.
3. Simplified astrocyte representations. Current network models incorporating astrocytes typically focus exclusively on excitatory gliotransmission (particularly glutamate) and neglect inhibitory GABAergic signaling from reactive astrocytes.

To understand the dynamic network mechanisms of epileptic seizure initiation and propagation in interacting neural and astrocytic networks, we developed a biologically relevant spiking neural network model that incorporates astrocytes. This model implements the transition from normal to epileptiform activity, including its spontaneous termination, without requiring manual parameter tuning or external stimulation. We took as a starting point our previous studies where we showed that a phenomenological scale-free network model of coupled Kuramoto phase oscillators under excitability resource constraints can generate the epileptic-seizure-related extreme synchronization events [25,26]. Through theoretical analysis and numerical simulation, we established that the appearance of switches is rooted in spatial self-organization and temporal self-similarity of the network's critical dynamics. In this paper, we enhance the model's biological plausibility by replacing Kuramoto oscillator with the Izhikevich model of a spiking neuron, and the phenomenological description of excitability resource consumption with the influence of reactive astrocytes on synaptic transmission. Using extensive numerical simulations, we demonstrate that the interplay between fast neuronal dynamics and the slower astrocyte-induced dynamic rearrangement of the neural network's functional architecture results in critical system behavior known as self-organized bistability. This self-organized dynamic regime is characterized by the spontaneous triggering of short-lived extreme synchronization events—a hallmark of epileptic seizure activity. The model generates trains of seizures, reproducing the distribution of intervals between seizures observed in neurophysiological experiments. We also show that gap junction connectivity within the astrocyte network plays a protective role against epileptic discharges.

2. Model details

The imbalance of inhibition and excitation in neuronal signal transmission has been widely considered a key trigger for epileptic seizures [7]. Studies in both human and experimental models of temporal lobe epilepsy have consistently demonstrated a reduction in GABAergic interneurons within the hippocampus, leading to diminished synaptic inhibition [42]. We focus on a scenario where inhibition surrounding the epileptic focus has already been disbalanced. Our focus is on the properties of astrocyte-induced modulation of excitatory synaptic transmission within the neuronal network of the epileptic focus. Highly connected hubs in brain networks are crucial for seizure propagation [6]. When inhibition is disrupted, these hubs become more synchronized and interconnected, allowing excessive neural activity to spread rapidly from the seizure focus throughout the brain [46,47]. We chose significantly heterogeneous scale-free (SF) network model because of its demonstrated ability to reproduce focal epilepsy network properties and its established association with epileptic seizures in previous modeling studies [48,49]. Our SF spiking neural network consists of synaptically coupled neurons (90% excitatory and 10% inhibitory neurons) modeled using the Izhikevich model [50].

Based on experimental data showing that astrocytes interact with multiple neurons, hundreds of dendrites, and thousands of synapses — thus having the ability to coordinate activity from neuronal ensembles — each astrocyte in our model bidirectionally interacts with five excitatory neurons [24]. Astrocytes, generating calcium signals, are connected by local gap junction diffusive couplings and interact with excitatory neurons via chemicals diffusing in the extracellular space. Hyperactivation of excitatory neurons during the onset of an epileptic seizure causes strong astrocytic Ca^{2+} signals, that are triggered by neurotransmitters released by neurons. Increased Ca^{2+} signaling induces the release of GABA into the extracellular space. GABA activates tonic $GABA_A$ receptor mediated currents in excitatory neurons and reduces seizure susceptibility, thereby apparently compensating for the loss of interneurons [43,44]. In the model we describe a compensatory anti-epileptic mechanism of astrocytic influence by Ca^{2+} mediated gliotransmission to curb epileptiform activity in pathological tissue. The scheme of the network topology is shown in Fig. 1.

2.1. Neural network

Among the existing biologically plausible neuron models, we chose the Izhikevich model [50] of membrane potential dynamics due to its computational efficiency in simulating large-scale networks while being able to reproduce the dynamics of almost all types of cortical neurons. The Izhikevich neuron model can be represented by the following system of differential equations [50]:

$$\begin{aligned} \frac{dV_i}{dt} &= 0.04V_i^2 + 5V_i - U_i + 140 + I_{\text{app,i}} + I_{\text{syn,i}};\\ \frac{dU_i}{dt} &= a(bV_i - U_i); \end{aligned} \tag{1}$$

with the auxiliary after-spike resetting

$$\text{if } V_i \geq 30 \text{ mV, then } \begin{cases} V_i \leftarrow c \\ U_i \leftarrow U_i + d, \end{cases} \tag{2}$$

where the subscript i corresponds to the neural index, V_i and U_i are dimensionless variables. Following [50], Eq. (1) was obtained by fitting the spike initiation dynamics of a cortical neuron so that the neuronal membrane potential V_i has mV scale and the time t has ms scale. The applied current $I_{\text{app,i}}$ simulates the input signal, $I_{\text{syn,i}}$ is the synaptic current.

As an input signal $I_{\text{app,i}}$, each neuron in the network received a direct current I_{DC} and Poisson noise. The Poisson noise was represented by a sequence of rectangular pulses with an amplitude I_{Poiss} and a duration t_{Poiss}. The inter-pulse interval was randomly selected from a Poisson distribution:

$$P(m) = \frac{\sigma^m}{m!}\exp^{-\sigma}, \tag{3}$$

where P is the probability, m is the number of events, and σ is the expectation value.

A SF network was chosen for the topology of synaptic connectivity in the neuronal network. SF networks are characterized by a distinct degree distribution exhibiting a power-law relationship: a small number of nodes, known as hubs, have a disproportionately high number of connections compared to the average. This power-law distribution of local cluster sizes reflects the structural self-similarity characteristic of SF networks. Another key feature of SF networks is their clustering coefficient distribution. This distribution also follows a power-law, indicating that nodes with fewer connections tend to be part of densely interconnected sub-networks. These sub-networks are connected to each other through the network's high-degree hubs. To generate SF topology in the network model, we used the Barabasi–Albert algorithm [51], where the network grows through preferential attachments.

The Barabási-Albert algorithm, while creating a SF graph, results in bidirectional connections between nodes. This differs from the unidirectional nature of chemical synapses in the brain. To align with biological reality, we modified the generated SF network by randomly removing one direction of each connection. Neuronal types were randomly assigned, with 90% of neurons in the network designated as excitatory and the remaining 10% as inhibitory.

The synaptic current, $I_{\text{syn,i}}$, of ith neuron represents the sum of all the currents received from its presynaptic neurons, averaged over the number of synapses, and is calculated according to the formula [52,53]:

$$I_{syn,i} = \frac{1}{N_{in,i}} \sum_{k=1}^{N_{in,i}} \frac{w_{syn,k}(E_{\text{syn}} - V_i)}{1 + \exp(-V_{\text{pre,k}}/k_{\text{syn}})}, \tag{4}$$

where $N_{in,i}$ is the total number of synapses, $w_{syn,k}$ is the weight of the kth synapse associated with the neuron (see Section 2.3). The weights of excitatory synapses are modified by the influence of astrocytes associated with a given neuron, whereas inhibitory synapse weights remain constant. V_{pre} is the membrane potential of the presynaptic neuron, E_{syn} is the synaptic reversal potential. Parameter k_{syn} denotes the steepness of synaptic activation function threshold. We neglect the synaptic and axonal delays in system for simplicity.

The descriptions of neural network parameters and their values can be found in Table 1.

2.2. Astrocytic network

The astrocytic network consists of A astrocytes connected via local diffusive coupling with nearest neighbors. We utilized the Ullah model [54] as a model for the calcium signalization of an astrocyte. This model is a system of differential equations that describes the dynamics of intracellular concentrations of two key active substances: calcium ions (Ca^{2+}) and inositol 1,4,5-trisphosphate (IP_3) molecules:

$$\begin{aligned} \frac{d[Ca^{2+}]_i}{dt} &= J_{\text{ER}} - J_{\text{pump}} + J_{\text{leak}} + J_{\text{in}} - J_{\text{out}} + J_{\text{Gca}};\\ \frac{dh_i}{dt} &= a_2\left(d_2\frac{[IP_3]_i + d_1}{[IP_3]_i + d_3}(1 - h_i) - [Ca^{2+}]_i h_i\right);\\ \frac{d[IP_3]_i}{dt} &= \frac{[IP_3]^* - [IP_3]_i}{\tau_{IP3}} + J_{\text{PLC}\delta} + J_{\text{glu}} + J_{\text{Gip3}} \end{aligned} \tag{5}$$

where i is the astrocyte index. The variables $[Ca^{2+}]$ and $[IP_3]$ are represent the concentrations of cytosolic calcium and IP_3, respectively. h is a fraction of activated IP_3 receptor on the endoplasmic reticulum (ER) membrane. J_{ER} is Ca^{2+} flux from the ER to the cytosol, J_{pump} is the pump flux from cytosol to ER, J_{leak} is the leakage flux from the ER to the cytosol. The fluxes J_{in} and J_{out} describe the exchange of

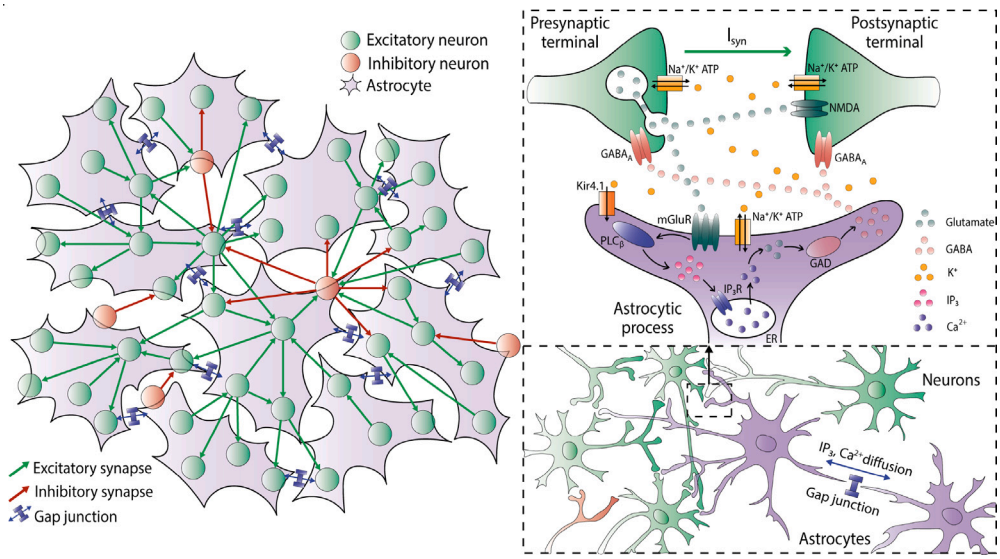

Fig. 1. Neuron-astrocyte network topology. Neurons within the network are connected according to the SF graph. The neural network consists of 90% excitatory and 10% inhibitory neurons. Excitatory neurons interact bidirectionally with nearby astrocytes through tripartite synapses. Glutamate released from the presynaptic excitatory neuron activates metabotropic glutamate receptors (mGluRs) on the astrocyte membrane. Metabotropic receptors are G-protein-coupled receptors that activate phospholipase C-β (PLC$_\beta$), leading to an increase in intracellular concentration of inositol 1,4,5-triphosphate (IP$_3$). IP$_3$ molecules diffuse to the endoplasmic reticulum (ER), where they bind to IP$_3$ receptor (IP3R) channels. This process results in the release of calcium from ER and an increase in cytosolic calcium concentration (calcium event). Epileptic activity induces GABA (gamma-aminobutyric acid) production in astrocytes. This process is mediated by the decarboxylation of glutamate by the enzyme glutamate decarboxylase (GAD). Upon release into the extracellular space, GABA activates extrasynaptic GABA$_A$ receptors on excitatory neurons, eliciting tonic inhibitory Cl^- currents. These currents subsequently attenuate neuronal excitability, contributing to the suppression of epileptic activity. Astrocytes are interconnected via gap junctions, which are permeable to IP$_3$ and Ca^{2+}.

calcium with the extracellular space. $J_{PLC\delta}$ describes the production of IP$_3$ by phospholipase Cδ (PLCδ), J_{glu} describes the glutamate-induced IP$_3$ production in response to neural activity (see Section 2.3). These fluxes are expressed as follows:

$$\begin{aligned}
J_{ER} &= c_1 v_1 [Ca^{2+}]^3 h^3 [IP_3]^3 \frac{\left(c_0/c_1 - (1+1/c_1)[Ca^{2+}]\right)}{\left(([IP_3]+d_1)([Ca^{2+}]+d_5)\right)^3};\\
J_{pump} &= \frac{v_3[Ca^{2+}]^2}{k_3^2+[Ca^{2+}]^2};\\
J_{leak} &= c_1 v_2 \left(c_0/c_1 - (1+1/c_1)[Ca^{2+}]\right);\\
J_{in} &= \frac{v_6[IP_3]^2}{k_2^2+[IP_3]^2};\\
J_{out} &= k_1[Ca^{2+}];\\
J_{PLC\delta} &= \frac{v_4\left([Ca^{2+}]+(1-\alpha)k_4\right)}{[Ca^{2+}]+k_4}.
\end{aligned} \tag{6}$$

Astrocytes interact with each other through gap junctions. Gap junctions are permeable to the IP$_3$ and to calcium ions [55,56]. Currents J_{Gca} and J_{Gip3} describe the diffusion of Ca^{2+} ions and IP$_3$ molecules via gap junctions of the ith astrocyte and can be expressed as follows:

$$\begin{aligned}
J_{Gca} &= d_{Ca}\sum_j([Ca^{2+}]_j - [Ca^{2+}]_i);\\
J_{Gip3} &= d_{IP3}\sum_j([IP_3]_j - [IP_3]_i);
\end{aligned} \tag{7}$$

where j, d_{Ca} and d_{IP3} represent, respectively, the number of astrocytes connected to the ith astrocyte and the Ca^{2+} and IP$_3$ diffusion rates. The biophysical interpretation of all parameters in Eqs. (5), (6), (7), as well as their respective values, can be found in [54]. A summary of these parameters, specifically related to the astrocytic network, is provided in Table 2. It is important to note that the timescale of the calcium dynamics model in astrocytes is in seconds, while the timescale of the Izhikevich model (Eqs. (1) and (2)) is in milliseconds. To ensure consistency in timescales within the combined model, the relevant model parameters were appropriately rescaled.

2.3. Bidirectional neuron-astrocyte interaction

Each astrocyte in the model bidirectionally interacts with ensemble of $N_A = 5$ neurons. Spiking neuronal activity leads to the release of the neurotransmitter glutamate from the presynaptic terminals into the synaptic gap. Once released, glutamate binds to the metabotropic glutamate receptors (mGluRs) located on the membrane of astrocytes. This binding event triggers the production of inositol 1,4,5-trisphosphate (IP$_3$) within the astrocytes. The production of IP$_3$ initiates the generation of a calcium pulse.

The amount of neurotransmitter-glutamate that diffuses from the synaptic cleft associated with the ith pyramidal neuron and reaches the astrocyte is described by the following equation [57,58]:

$$\frac{dG_i}{dt} = -\alpha_{glu}G_i + k_{glu}H\left(V_i - 30\text{ mV}\right), \tag{8}$$

where α_{glu} is the glutamate clearance constant, k_{glu} is the release efficiency, H is the Heaviside step function, and V_i is the membrane potential of ith pyramidal neuron. Glutamate contacts the mGluRs on the astrocyte membrane and initiates the production of IP$_3$. The flux J_{glu} represents the glutamate-induced IP$_3$ production and is defined as follows:

$$J_{glu} = \begin{cases} imp_{glu}\sum_{i=1}^{N_A} G_i, & \text{if } \sum_{i=1}^{N_A} G_i > G_{thr},\\ 0, & \text{otherwise;}\end{cases} \tag{9}$$

where the parameter G_{thr} is the threshold for glutamate, imp_{glu} is the mGluRs sensitivity coefficient.

It has been shown that reactive astrocytes aberrantly overproduce GABA through de novo synthesis and or decarboxylation of excess glutamate [43,44]. Astrocytes in epileptic focus exhibit a tonic release of GABA, presumably through Bestrophin−1 channels [43]. Bestrophin−1 channels are Ca^{2+} activated anion channels, and increased GABA release could hence be a downstream effect of increased Ca^{2+} signaling in reactive astrocytes [59]. Upon release into the extracellular space, GABA activates extrasynaptic GABA$_A$ receptors on excitatory neurons

Table 1
Neural network parameters [50,52].

Parameter	Parameter description	Value
N	total number of neurons	1000
	number of excitatory neurons	900
	number of inhibitory neurons	100
	The dynamics of the membrane potential of a single neuron	
a	time scale of the recovery variable	0.02
b	sensitivity of the recovery variable to the sub-threshold fluctuations of the membrane potential	0.2
c	after-spike reset value of the membrane potential	−65 mV
d	after-spike reset value of the recovery variable	8
	Input signal	
I_{DC}	amplitude of a direct current (DC)	2.5 μA
I_{Poiss}	amplitude of Poisson noise pulses	7 μA
t_{Poiss}	duration of Poisson noise pulses	3 ms
σ	mathematical expectation (average interval between pulses)	100 ms
	Synaptic current	
n_0	SF existing nodes	6
n	SF new edges	6
E_{syn}	synaptic reversal potential for excitatory synapses	0 mV
	synaptic reversal potential for inhibitory synapses	−90 mV
k_{syn}	steepness of the synaptic activation function	0.2 mV
w_{syn0}	maximum weight of the excitatory synapse	4.05 mS
w_{syn}	weight of the inhibitory synapses	3 mS

Table 2
Astrocyte network parameters [54].

Parameter	Parameter description	Value
A	number of astrocytes	200
c_0	total Ca^{2+} in terms of cytosolic volume	2.0 μM
c_1	(ER volume)/(cytosolic volume)	0.185
v_1	max Ca^{2+} channel flux	6 s^{-1}
v_2	Ca^{2+} leak flux constant	0.11 s^{-1}
v_3	max Ca^{2+} uptake	2.2 μM s^{-1}
v_6	maximum rate of activation dependent calcium influx	0.2 μM s^{-1}
k_1	rate constant of calcium extrusion	0.5 s^{-1}
k_2	half-saturation constant for agonist-dependent calcium entry	1 μM
k_3	activation constant for ATP-Ca^{2+} pump	0.1 μM
d_1	dissociation constant for IP_3	0.13 μM
d_2	dissociation constant for Ca^{2+} inhibition	1.049 μM
d_3	receptor dissociation constant for IP_3	943.4 nM
d_5	Ca^{2+} activation constant	82 nM
α		0.8
v_4	max rate of IP_3 production	0.3 μM s^{-1}
$1/\tau_{IP3}$	rate constant for loss of IP_3	0.14 s^{-1}
$[IP_3]^*$	steady state concentration of IP_3	0.16 μM
k_4	dissociation constant for Ca^{2+} stimulation of IP_3 production	1.1 μM
d_{Ca}	Ca^{2+} diffusion rate	0.005 s^{-1}
d_{IP3}	IP_3 diffusion rate	0.005 s^{-1}

and elicits tonic inhibitory Cl^- currents, which attenuates neuronal excitability. We model this process of astrocytic modulation of neuron excitability and synaptic transmission using a phenomenological description in the following form. The strength of the excitatory synaptic input connection w_{syn} for the neuron interacting with the astrocyte decreases proportionally to the amplitude of the calcium pulse in the astrocyte. This astrocytic regulation of excitatory synaptic transmission is described in the model as follows:

$$\frac{dw_{syn}}{dt} = \alpha_w(w_{syn0} - w_{syn}) - \beta_w[Ca^{2+}], \tag{10}$$

where α_w is a rate of synaptic connection strength recovery, β_w is a strength of astrocytic influence on synaptic transmission, w_{syn0} is maximum synaptic weight, $[Ca^{2+}]$ represents the intracellular calcium concentration in the astrocyte.

Model equations are integrated using the Euler method with a fixed time step, $\Delta t = 0.1$ ms [50]. A detailed listing of model parameters and values can be found in Table 1 (Neural network parameters), Table 2 (Astrocyte network parameters), and Table 3 (Neuron-astrocyte interaction parameters).

3. Global instantaneous order parameter

To assess the degree of synchronization of neuronal dynamics in the network, we computed the global instantaneous order parameter, $S(t)$, according to the formula [60,61]:

$$S(t) = \frac{1}{N(N-1)} \sum_{i \neq j} cos^2\left(\frac{\phi_i(t) - \phi_j(t)}{2}\right), \qquad \phi_i(t) = 2\pi\left(t - t_i^k\right) / \left(t_i^{k+1} - t_i^k\right), \tag{11}$$

where t is the time in ms, N is the size of the neural network, $\phi_i(t)$ and $\phi_j(t)$ are the instantaneous phases of the ith and jth neurons in the network, respectively, at time t; $i, j \in [1, N]$ are the indices of the neurons in the network. t_i^k and $t_i^{(k+1)}$ are the time moments of the kth and $(k+1)^{th}$ membrane potential spikes of the neuron.

A value of $S = 1$ corresponds to complete synchronization of the entire network, while $S = 0.5$ corresponds to complete asynchrony of the network dynamics.

Table 3
Neuron-astrocyte interaction parameters [57].

Parameter	Parameter description	Value
N_A	number of neurons interacting with one astrocyte	5
α_{glu}	glutamate clearance constant	10 s^{-1}
k_{glu}	efficacy of the glutamate release	100 s^{-1}
imp_{glu}	mGluRs sensitivity coefficient	167
G_{thr}	threshold concentration of glutamate for IP_3 production	0.044
$[Ca^{2+}]_{\text{thr}}$	threshold concentration of Ca^{2+} for the astrocytic modulation of synapse	0.2 μM
α_w	strength of the astrocyte-induced modulation of synaptic weight	0.01 s^{-1}
β_w	strength of the astrocyte-induced modulation of synaptic weight	0.02 mS s^{-1} μM^{-1}
τ_{astro}	duration of the astrocyte-induced modulation of synapse	5 s

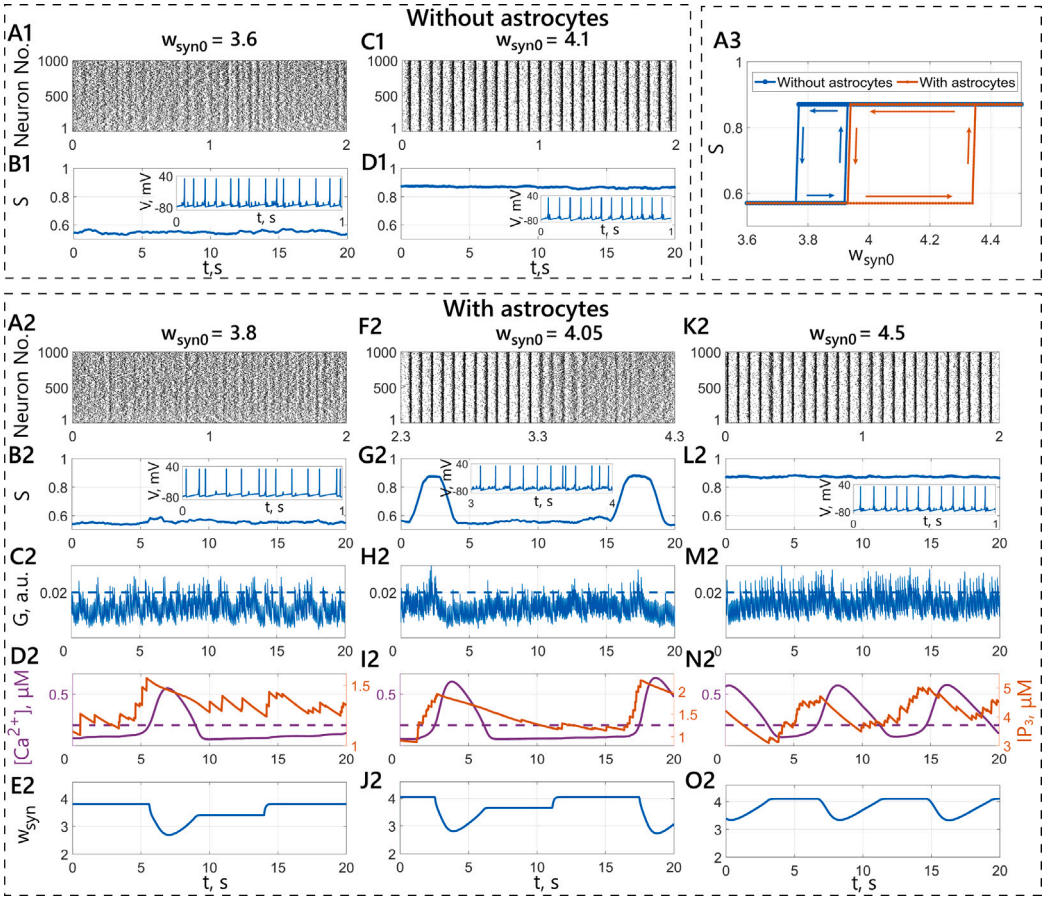

Fig. 2. (A1–D1) Dynamics of the global order parameter in a spiking neuron-astrocyte network without astrocytic modulation of synaptic transmission. The network's behavior across different synaptic connection weights: (A1–B1) is for w_{syn0} = 3.6, while (C1–D1) shows results for w_{syn0} = 4.1. (A1, C1) – spike raster of neurons; (B1,D1) – global instantaneous order parameter S, which quantifies the synchronization level of the neuronal network, and representative trace of the membrane potential V dynamics of a single neuron within the network. (A2–O2) Dynamics of the global order parameter in a spiking neuron-astrocyte network with modulation of excitatory synaptic transmission by astrocytes. The network's behavior across different synaptic connection weights: (A2–E2) is for w_{syn0} = 3.8, (F2–J2) – w_{syn0} = 4.05, and (K2–O2) – w_{syn0} = 4.5. (A2, F2, K2) – spike raster of neurons; (B2,G2,L2) – global instantaneous order parameter S, and representative trace of the membrane potential V dynamics of a single neuron within the network; (C2,H2,M2) – extracellular concentration of neurotransmitter G released by this neuron; (D2,I2,N2) – intracellular calcium concentration $[Ca^{2+}]$ and IP_3 concentration in the astrocyte; (E2,J2,O2) – synaptic weight w_{syn}. (A3) presents the bifurcation diagrams for S. This diagram maps the network's behavior as the maximum synaptic connection weight (w_{syn0}) is varied.

4. Results

We begin by analyzing the model in the absence of astrocytic modulation of synaptic transmission. Next, we demonstrate how astrocytic modulation can dynamically switch the model between synchronous and asynchronous states. We will then move on to explore the role of astrocytes in timing imbalances during extreme synchronization events and the detailed dynamics of neural spikes. Finally, we will analyze the statistics of durations between consecutive instances of epileptic seizures.

4.1. The influence of reactive astrocytes on the synchronization of neural network signaling

We first examine the dynamics of our neuron-astrocyte network model in the absence of astrocytic influence on synaptic transmission efficiency. In this case, Eq. (10) yields $w_{syn} = w_{syn0}$. The upper panel of Fig. 2 illustrates neural network signaling for weak and strong excitatory synaptic couplings. In case of weak excitatory synaptic weights (w_{syn0} = 3.6) the neural network exhibits asynchronous activity (Fig. 2A1) with a low value of the global order parameter ($S \approx 0.5$, Fig.

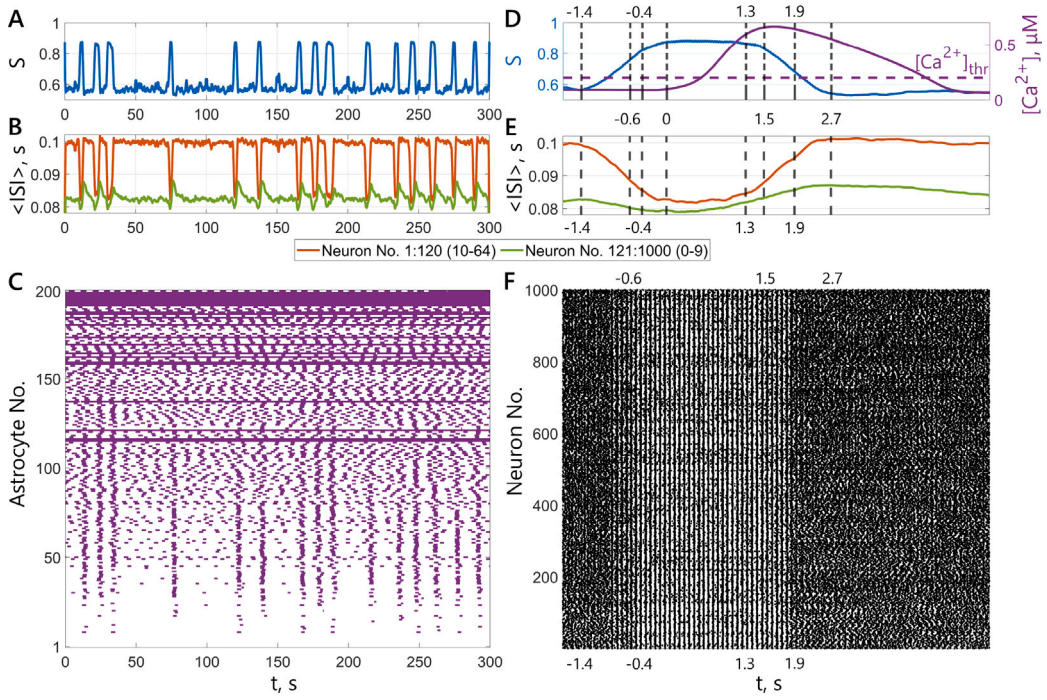

Fig. 3. Extreme synchronization events. The plots are obtained for w_{syn0} = 4.05. (A–C) – long simulation time interval (300 s) and (D–F) — single event. (A,D) – global instantaneous order parameter $S(t)$; (B,E) – average interspike intervals (ISI) for two distinct neuronal populations: highly connected and low-connected neurons; (C) – calcium events in astrocytes; (F) – spike raster of neurons.

2B1). With an increase in the weights of excitatory synaptic connections (w_{syn0} = 4.1), synchronization is observed in the signaling of the neural network, with $S \approx 0.9$ (Fig. 2C1,D1). To analyze the transition between these two dynamical states of the modeled neural network as a function of excitatory synaptic strength, we constructed a one-parameter bifurcation diagram (Fig. 2A3, blue curve), which reflects the dependence of the global order parameter on the excitatory synaptic strength. The diagram reveals hysteresis in the range $3.77 \leq w_{syn0} \leq 3.92$. The network exhibits an abrupt transition to coherence, known as a first-order transition or explosive synchronization [62]. Our results are consistent with the previous studies in network dynamics of neuron-like oscillators [25,26,63,64]. For values of $w_{syn0} < 3.77$, only an asynchronous regime is observed ($S \approx 0.5$), while for $w_{syn0} > 3.92$, a synchronous regime is possible ($S \approx 0.9$).

Next, we incorporated the influence of reactive astrocytes on excitatory synaptic transmission and investigated its effect on synchronization in the neuron-astrocyte network model (Fig. 2, lower panel). Astrocytic modulation of synaptic transmission was activated through the following mechanism: Neuronal action potential generation elevates extracellular glutamate concentration (G; Fig. 2 C2,H2,M2). When G exceeds a threshold value (G_{thr}), it triggers transient, rapid increases in astrocytic intracellular IP_3, ultimately leading to calcium impulses (Fig. 2 D2,I2,N2). Astrocytic activation (characterized by exceeding the intracellular calcium threshold, $[Ca^{2+}]_{thr}$) temporarily suppresses excitatory synaptic weights (Fig. 2 E2,J2,O2). This astrocytic regulation shifts the hysteresis towards larger values of the maximum connection weight (w_{syn0}) and expands it on the one-parameter bifurcation diagram of the global order parameter (Fig. 2A3). Combined with the bistability region in our model, astrocytic modulation of excitatory synaptic transmission enables spontaneous transitions between synchronous and asynchronous modes when w_{syn0} lies within the hysteresis region. By varying the maximal excitatory synaptic strength (w_{syn0}), we identified three signaling modes in the neuron-astrocyte network model: asynchronous regime for weak coupling ($w_{syn0} < 3.94$), synchronous regime for strong connectivity ($w_{syn0} > 4.34$) and astrocyte-driven switching regime ($3.94 < w_{syn0} < 4.34$), characterized by transitions between synchronization and desynchronization. The self-organized dynamic regime — marked by spontaneous, short-lived extreme synchronization events — is proposed to represent epileptic seizure activity. Notably, the duration of these events increases with higher values of w_{syn0}.

By modeling neuron-astrocyte interactions at various values of four key parameters (w_{syn0}, α_w, β_w, imp_{glu}), we were able to identify parameter ranges within our model that support the spontaneous emergence of explosive synchronization:

$$3.94 < w_{syn0} < 4.34, \quad 0.01 < \alpha_w < 0.02,$$
$$33 < imp_{glu} < 180, \quad 0.008 < \beta_w < 0.03.$$

When investigating the effect of varying a single parameter, the remaining ones were held constant according to the values specified in Table 3.

4.2. Self-organized bistability in a spiking neural network with reactive astrocytes

To assess the interplay between neuronal and astrocytic dynamics during the initiation and termination of spontaneous extreme synchronization events, we analyzed their activity in detail. Given the scale-free (SF) topology of our neural network — characterized by a heterogeneous distribution of connections where a small fraction of nodes (hubs) possess disproportionately high connectivity compared to average nodes — we compared the dynamics of average interspike intervals (ISI; Fig. 3B,E) between two neuronal populations: 120 highly connected neurons (≥ 10 couplings) and 880 low-connected neurons (0–10 couplings), relative to the global order parameter during synchronization events. During synchronous events (Fig. 3F), highly connected neurons exhibited a pronounced ISI decrease, from 100 to 83 ms, whereas low-connected neurons showed a smaller reduction, from 83 to 79 ms (Fig. 3E). Notably, in the latter group, spiking frequency decreased further within 5 s post-synchronization, consistent with astrocyte-mediated suppression of excitatory synaptic weights (Fig. 3B,E). To investigate astrocytic contributions, we generated a raster plot of astrocyte activity (Fig. 3C), marking intervals of intracellular calcium threshold exceedance ($[Ca^{2+}]_{thr}$ = 0.2) in purple.

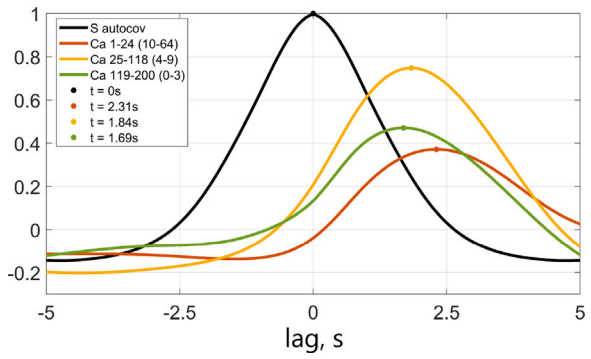

Fig. 4. Correlation analysis between the global instantaneous order parameter, $S(t)$, and calcium signals for individual groups of astrocytes.

Astrocytes were ranked by decreasing node degree (based on their associated excitatory neuronal ensemble's total connections), enabling direct comparison with S (Fig. 3A,C). A strong correlation emerged: synchronous astrocyte activity — especially in astrocytes coupled to the most highly connected neurons — coincided with sharp rises in S (peak $S \approx 0.9$). Mirroring the neuronal activity-frequency gradient, astrocytes in the raster's lower tiers displayed low-frequency calcium signals.

To investigate the influence of the synchronous regime on astrocyte dynamics, we conducted a correlation analysis between the S index and calcium signals for individual groups of astrocytes (Fig. 4). Our analysis revealed that the average Ca^{2+} signal of astrocytes associated with the 24 most highly connected neurons ($\geq$ 10 couplings) showed a peak correlation coefficient with S at a time delay of 2.31 s. As neuronal connectivity decreased, this delay diminished slightly: 1.84 s for astrocytes linked to neurons with 4–9 couplings (astrocytes 25–118); 1.69 s for astrocytes connected to neurons with 0–3 couplings (astrocytes 119–200). Notably, astrocytes associated with neurons of intermediate connectivity (4–9 couplings) exhibited the highest correlation amplitude, suggesting their activity most closely mirrors the dynamics of synchronization episodes.

These findings demonstrate that an increase in the synchrony of neuronal spiking is accompanied by a transition to a higher spiking rate, leading to the release of the neurotransmitter glutamate. Consequently, this glutamate release triggers a rise in intracellular Ca^{2+} above the threshold level $[Ca^{2+}]_{thr}$ (Fig. 3D). This elevated calcium level, in turn, suppresses neurotransmitter release and reduces the flow of synaptic current, ultimately disrupting synchronous discharge. This suppression of extreme synchronization occurs at an average time interval of 1.38 s after calcium reaches its threshold value.

4.3. Synchronization process: microscopic dynamics

To elucidate the mechanism underlying neuronal synchronization, we meticulously examined the ISI distributions during the transition period from the fully asynchronous regime to the initial point of the epileptic seizure. Fig. 3D depicts the key timings during a single event. Subsequently, Fig. 5 diagrams chronologically illustrate the evolution of ISI distributions. The horizontal axis represents the parameter r_i, which reflects the individual order parameter of the ith neuron, calculated based on its connected neurons according to the formula: $r_i = 1/N_{in,i} | \sum_{j=1}^{N_{in,i}} B_{ij} e^{\theta_j} |$, where B is the adjacency matrix of synaptic connections in the network: $B_{ij} = 1$ determines the presence of a connection between the ith and jth neurons, and the connection is absent if $B_{ij} = 0$; θ_j is phase of the jth neuron; N_{in} is the total number of incoming synaptic connections. When the parameter $r_i = 1$, the local neuron exhibits complete phase synchrony with its immediate neighbors, conversely, $r_i = 0$ indicates complete desynchronization.

Fig. 5A–D reveals that as we approach $t = 0$, where S reaches its maximum, the coefficients r_i migrate towards 1, indicating increased synchrony, and the deviation of ISI becomes smaller. Furthermore, the second process precedes the first one. This suggests that during the formation of an extreme synchronization event, neurons initially attain a high firing rate. Subsequently, under the influence of synaptic connections, neurons fine-tune their firing patterns, minimizing mutual delays. Importantly, this process is independent of the number of connections, implying a consistent neuronal behavior across different connectivity levels. The reverse process of synchronization destruction unfolds in a mirror image (Fig. 5E–H). Initially, neurons lose connections with their neighbors, remaining in the high spiking rate mode for a period of time (the distribution of indices r_i shifts to the left from 1). Subsequently, the deviation of ISI increases, eventually leading to a completely asynchronous state.

To understand the contribution of inhibitory neuron activity and the influence of biologically plausible neuron-astrocyte interactions — where astrocytes integrate signals from neuronal ensembles — in generating epileptiform spontaneous extreme synchronization events in our spiking neuro-astrocytic network model, we present numerical simulations of a simplified network model in the Appendix. This simplified model lacks inhibitory neurons and features astrocytes interacting with single neurons rather than ensembles. A comparative analysis reveals that the simplified model also exhibits a self-organized bistable regime with spontaneous generation of short-lived extreme synchronization events. The absence of inhibitory neurons leads to more precise spike synchronization during epileptiform activity, with global order parameter values reaching higher magnitudes ($S \approx 1$) compared to the full network model discussed in the main text ($S \approx 0.9$). Similarly, astrocytes interacting bidirectionally with only one neuron show more correlated calcium activity. However, such near-absolute synchronization in both neural and astrocytic networks is not observed in experimental *in vivo* recordings from animal models of epilepsy [17,45], suggesting that the simplified model may overestimate synchronization dynamics.

4.4. Impact of IP_3 and Ca^{2+} diffusion in astrocyte gap junctions on neuronal network dynamics

Loss of astrocytic gap junction coupling has been identified as a key factor in the initiation and progression of epileptic seizures [33]. Partial or complete blockage of gap junctions disrupts astrocyte network connectivity, leading to impaired propagation of Ca^{2+} waves throughout the astrocyte network. This can also result in neuronal network hyperactivity due to disruptions in K^+ and neurotransmitter homeostasis [33,36]. According to experimental data, in the absence of pathologies, the diffusion rates of IP_3 and Ca^{2+} through gap junctions between adjacent astrocytes are 0.01–1 s^{-1} and 0.015–0.03 s^{-1}, respectively [54]. In our study, epileptiform activity was observed at significantly lower diffusion rates ($d_{IP3} = 0.005$ s^{-1}, $d_{Ca} = 0.005$ s^{-1}), consistent with astrocyte pathology. Upon increasing the diffusion rates of IP_3 and Ca^{2+} in the model to values corresponding to healthy astrocytes (while maintaining other parameters constant), the neuronal network exhibited a stable asynchronous mode, and spontaneous brief transitions to synchronous mode were eliminated.

4.5. Comparing extreme synchronization events and epileptic animal EEG recordings

To complete our analysis of the spiking neuron-astrocyte network model, we investigated the distribution of return intervals between consecutive synchronization events. We simulated the model over an extended period and constructed a histogram of the distribution of time intervals between neighboring synchronization events on a bi-logarithmic scale. We then performed a linear fit to the obtained data. The Pearson's χ^2-test was employed to assess the agreement between the observed and expected power-law distributions. We analyzed the resulting distributions as a function of two key model parameters: the

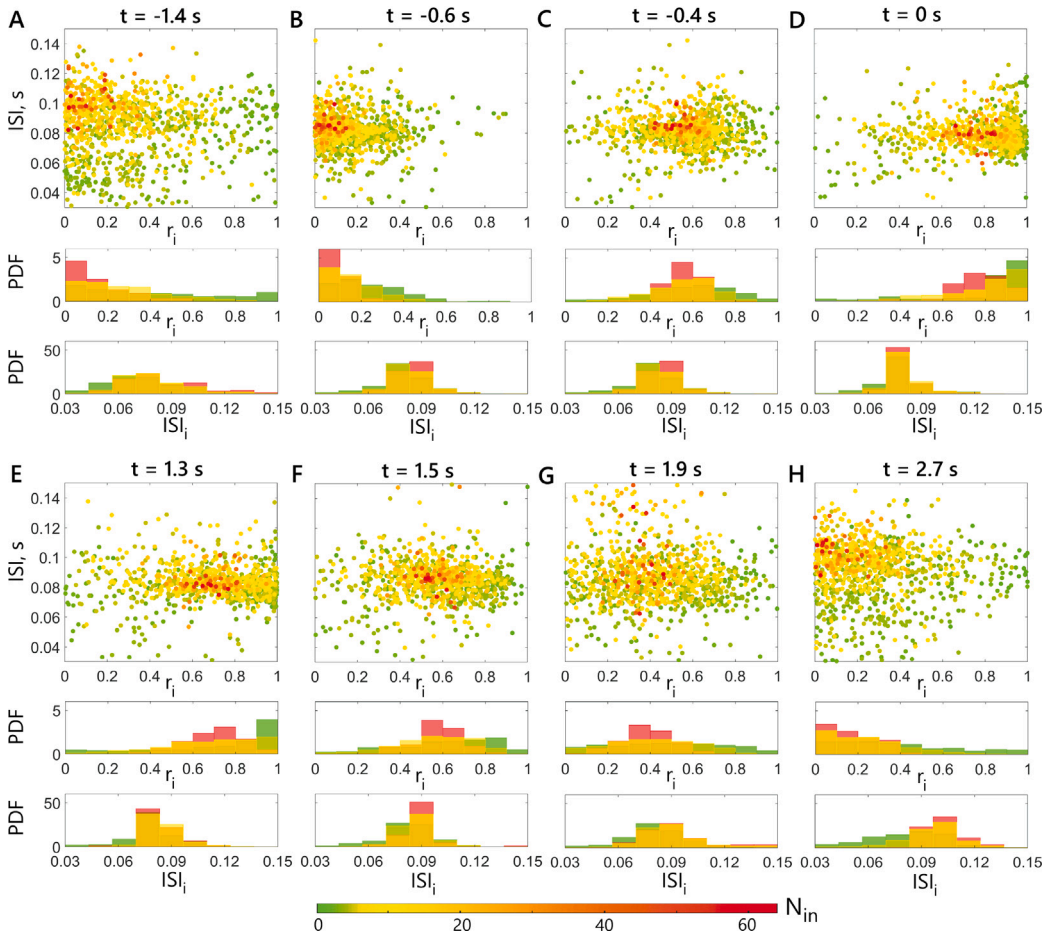

Fig. 5. The emergence and suppression of an extreme synchronization through the analysis of interspike intervals (ISI) data: (A–D) – the onset of an event in the time interval 1.4 s prior to the peak of the order parameter S, (E–H) – the breakdown of synchrony. Each point on these diagrams represents a specific neuron, and its color corresponds to N_{in}, the total number of incoming connections. Beneath each diagram are the corresponding ISI and the r_i index distributions. PDF is probability density function. During the initiation of synchrony, ISIs coalesce into a narrow band of values, after that one can see the alignment of spiking phases and the progression of individual r_i indices towards 1. Conversely, during the suppression of the synchronous mode, this process reverses. Notably, the ISI behavior of neurons with different connectivity levels does not exhibit statistically significant differences.

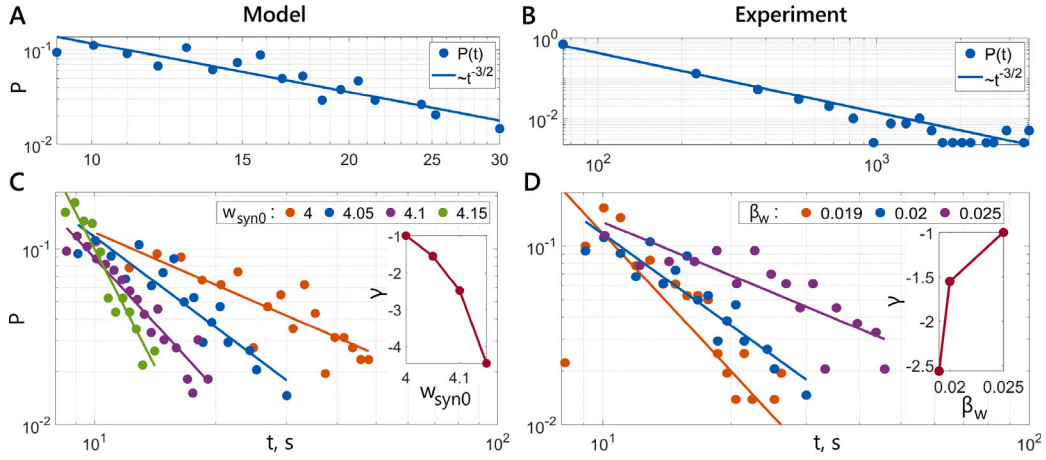

Fig. 6. (A) – Distributions of return intervals between consecutive synchronization events. Circles represent the observed distributions P(t), and solid lines show respective power-law fits $\sim e^{\gamma t}$. (B) – Averaged statistics of time periods between the EEG hallmarks of absence epilepsy in rats [65]. (C) – Distributions of return intervals between consecutive synchronization events for different w_{syn0}: 4 (χ^2 = 0.53, χ^2_{crit} = 28.87, *p-value* = 1, Sample size = 372); 4.05 (χ^2 = 0.32, χ^2_{crit} = 26.3, *p-value* = 1, Sample size = 561); 4.1 (χ^2 = 0.26, χ^2_{crit} = 27.59, *p-value* = 1, Sample size = 664); 4.15 (χ^2 = 0.19, χ^2_{crit} = 19.68, *p-value* = 1, Sample size = 644). The inset shows scaling exponent γ vs w_{syn0}. (D) – Distributions of return intervals between consecutive synchronization events for different β_w: 0.019 (χ^2 = 1.89, χ^2_{crit} = 27.59, *p-value* = 0.99, Sample size = 582); 0.02 (χ^2 = 0.32, χ^2_{crit} = 26.3, *p-value* = 1, Sample size = 561); 0.025 (χ^2 = 0.53, χ^2_{crit} = 25, *p-value* = 1, Sample size = 364). The inset shows scaling exponent γ vs β_w.

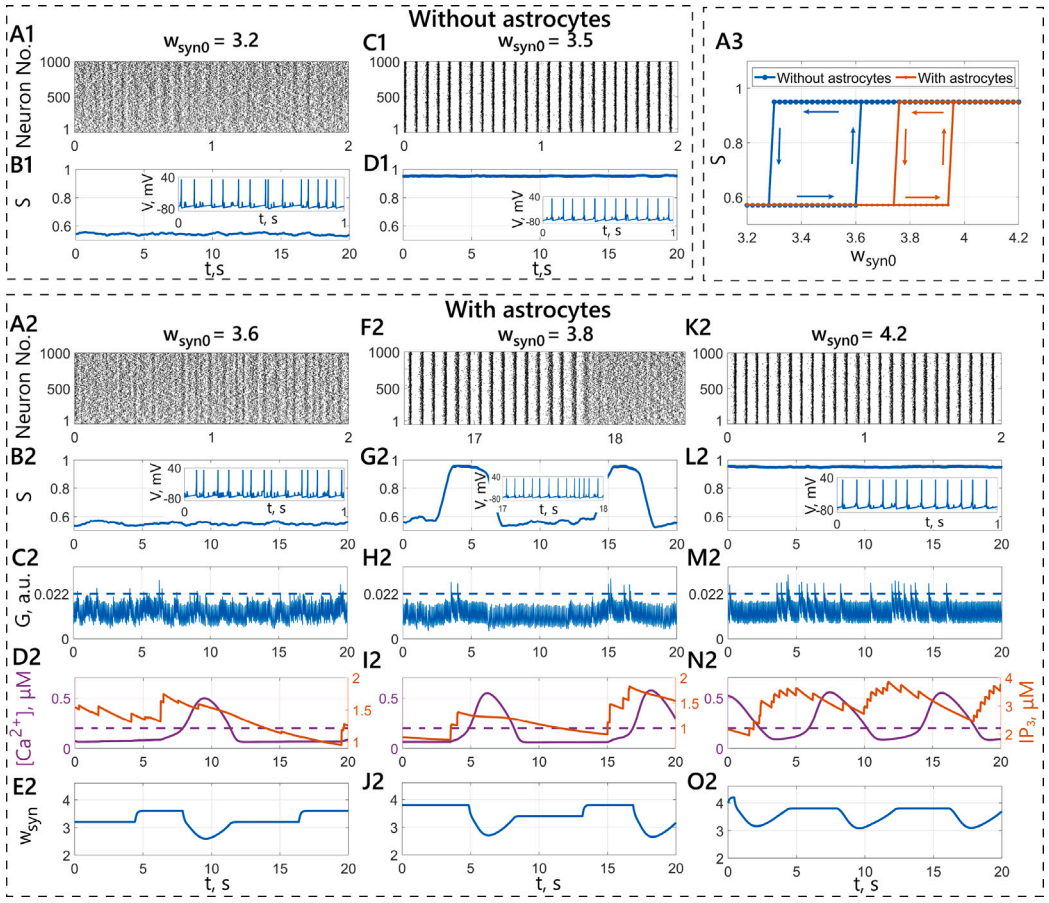

Fig. A.7. (A1–D1) Dynamics of the global order parameter in a spiking neuron-astrocyte network without astrocytic modulation of synaptic transmission. The network's behavior across different synaptic connection weights: (A1–B1) is for w_{syn0} = 3.2, while (C1–D1) shows results for w_{syn0} = 3.5. (A1,C1) – spike raster of neurons; (B1,D1) – global instantaneous order parameter S, which quantifies the synchronization level of the neuronal network, and representative trace of the membrane potential V dynamics of a single neuron within the network. (A2–O2) Dynamics of the global order parameter in a spiking neuron-astrocyte network with modulation of synaptic transmission by astrocytes. The network's behavior across different synaptic connection weights: (A2–E2) is for w_{syn0} = 3.6, (F2–J2) – w_{syn0} = 3.8, and (K2–O2) – w_{syn0} = 4.2. (A2, F2, K2) – spike raster of neurons; (B2,G2,L2) – global instantaneous order parameter S, and representative trace of the membrane potential V dynamics of a single neuron within the network; (C2,H2,M2) – extracellular concentration of neurotransmitter G released by this neuron; (D2,I2,N2) – intracellular calcium concentration $[Ca^{2+}]$ and IP_3 concentration in the astrocyte; (E2,J2,O2) – synaptic weight w_{syn}. (A3) presents the bifurcation diagrams for S. This diagram maps the network's behavior as the maximum synaptic connection weight (w_{syn0}) is varied.

maximum synaptic weight (w_{syn0}), shown in Fig. 6C, and the strength of astrocyte-induced modulation of synaptic weight (β_w), shown in Fig. 6D. Our findings reveal a significant influence of these parameters on the slope of the return interval distribution (scaling exponent γ). Increased synaptic connection weight leads to scaling exponent γ decrease (Fig. 6C), while increased astrocytic influence, conversely, increased γ (Fig. 6D).

For statistical comparison with experimental epilepsy data, we analyzed inter-event intervals from both our neuron-astrocyte network model and EEG-recorded seizure patterns in WAG/Rij rats - a validated genetic model of absence epilepsy [65]. The study utilized one-year-old male WAG/Rij rats with epidural electrodes implanted over the frontal cortex (site of maximal spike-wave discharge [SWD] amplitude), along with cerebellar reference and ground electrodes. Continuous wavelet transform (CWT) was used to represent the EEG signal with high temporal and frequency resolution, enabling differentiation of activity bursts from the remaining EEG. The authors analyzed the distribution of time periods (L) between adjacent SWD events. Their results showed that the L-interval distributions of SWDs were best approximated by a power law with an exponent of −3/2 in all individuals (Fig. 6B). Interestingly, we also observed a power-law dependence of the form $P(t) = t^{-3/2}$ (Fig. 6A), with model parameters w_{syn0} = 4.05 and β_w = 0.02, aligning with empirical observations of epileptic activity in rodent brains [65–68] (Fig. 6B). These studies demonstrate the extreme properties of both seizure amplitudes and temporal scaling, both governed by the -3/2 power law.

5. Discussion

Modeling epilepsy with dynamic models of spiking neural networks in isolation from their surrounding multi-component environment inherently presents an incomplete picture. We present a biologically relevant spiking neuron-astrocyte network model and demonstrate how hypersynchronous bursts can be effectively suppressed by the activation of so-called reactive astrocytes. The mathematical model represents a two-component network composed of interacting neuronal and astrocytic layers. The Izhikevich model was used to model spiking neurons, which were synaptically coupled according to a degree distribution. Astrocytes, interacting locally via gap junctions, were described by Ullah's model of intracellular calcium dynamics and activated by glutamate diffusing from neuronal synapses. Reactive astrocytes, stimulated by calcium elevation, provided feedback to the neuronal layer by releasing GABA. In constructing this feedback, we simulated the activation of $GABA_A$ synaptic receptors by the astrocytic GABA release. At the network level, our model demonstrated that the interplay between fast neuronal dynamics and the slower astrocyte-induced dynamic rearrangement of the neural network's functional architecture results

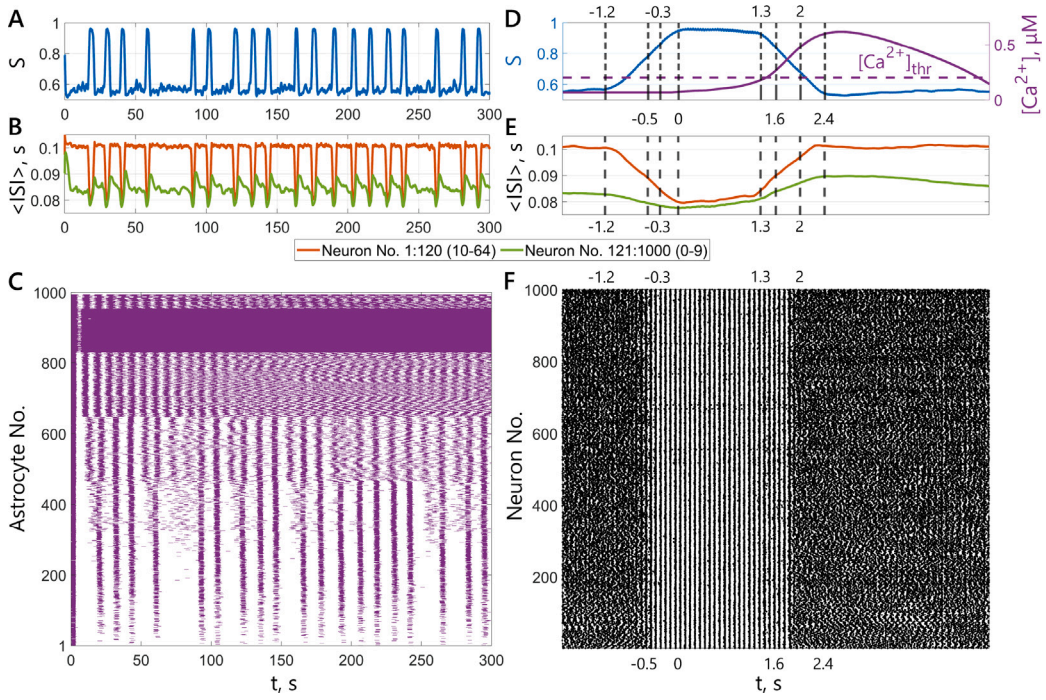

Fig. A.8. Extreme synchronization events. The plots are obtained for w_{syn0} = 3.8. (A–C) – long simulation time interval (300 s) and (D–F) - single event. (A,D) – global instantaneous order parameter $S(t)$; (B,E) – average interspike intervals (ISI) for two distinct neuronal populations: highly connected and low-connected neurons; (C) – calcium events in astrocytes; (F) – spike raster of neurons.

in critical system behavior known as self-organized bistability. This dynamic regime is characterized by the spontaneous triggering of short-lived, extreme synchronization events related to epileptic seizures. Interestingly, the model demonstrated a scale-free distribution of hypersynchronous burst appearance, similar to experimental studies of absence epilepsy.

Our model represents a local neuron-astrocyte network from an epileptic focus. It is established that epileptogenesis involves interactions across macroscopic neuronal and astrocytic populations, as well as entire brain structures. Remarkably, the statistical properties of interictal interval durations observed in our large-scale yet local networks match those of whole-brain EEG-recorded seizure characteristics. This finding suggests that epileptic discharge generation may be connected with local network-intrinsic mechanisms which subsequently propagate to brain-wide scales.

Similar to our study, many mathematical models incorporating astrocytes have shed light on their potential roles in epileptic neuronal activity, focusing on both single neurons [27–31] and networks [36–41]. These models investigate the impact of astrocytic glutamate release and uptake on neuronal dynamics, showing that increased astrocytic influence, particularly during glutamate release and binding to NMDA receptors, can lead to high-frequency neuronal firing [27,28]. Disruptions in potassium buffering by astrocytes [30,38] and impaired function of the astrocytic Na^+–K^+-ATP pump [31] can also contribute to neuronal depolarization and epileptic discharges.

Theoretical research on epilepsy in neuron-astrocyte networks highlights the roles of IP_3 diffusion [36,37], astrocytic potassium buffering [30,38], and influence on synaptic transmission [39–41] in seizure spread and termination. In a small network model, increasing the connectivity and diffusion rate within astrocytic networks, by increasing the number of gap junctions permeable to IP_3 molecules, inhibits the induction and spread of epileptic seizures [36]. This effect is achieved by reducing the frequency of Ca^{2+} oscillations in astrocytic network, leading to decreased glutamate release and a return to normal neuronal activity.

However, models of epilepsy fall short in comprehensively representing the complex interplay between astrocytic networks and neuronal activity. Specifically, they often struggle to accurately capture the mechanisms of seizure termination [36] and propagation [37], particularly regarding the dynamic interplay between astrocytic calcium waves and neuronal activity, including via gap junctions [36,37]. Moreover, existing models lack a comprehensive understanding of the intricate relationship between astrocytic K^+ buffering and neuronal excitability, which plays a crucial role in the initiation and spread of epileptic seizures [30,38].

The limitations of our proposed model can be attributed to the following key aspects. Firstly, the spiking neuron-astrocyte network model is influenced by the well-established experimental observation that epileptic seizures occur in brain regions with structural hubs. In essence, the SF topology is driven by the desire to create centers of activity through which synchronization processes are induced within the network. However, in a real brain, the prerequisites for the formation of a neural network graph and its spatial structure may differ significantly from our model.

Secondly, our model simplifies neuronal interactions by neglecting axonal delays, which play a significant role in the temporal dynamics of neural networks. Axonal delays can influence synchronization patterns and the propagation of epileptiform activity, potentially altering the onset, duration, or termination of seizures. Incorporating these delays would provide a more biologically accurate representation of network behavior and could reveal additional mechanisms underlying seizure dynamics.

Future research holds several promising avenues for enhancing the biological plausibility of epilepsy models. Recent studies have demonstrated that optogenetic activation of astrocytes can effectively reduce seizures, not through calcium signaling, but by promoting their K^+ buffering via the Na^+–K^+-ATPase pump [17]. This mechanism, by regulating K^+ levels, specifically inhibits hyperactive neurons, contributing to the cessation of seizures. Furthermore, other experimental work highlights the critical role of glia in seizure initiation, revealing that generalized seizures arise from the massive release of glutamate into

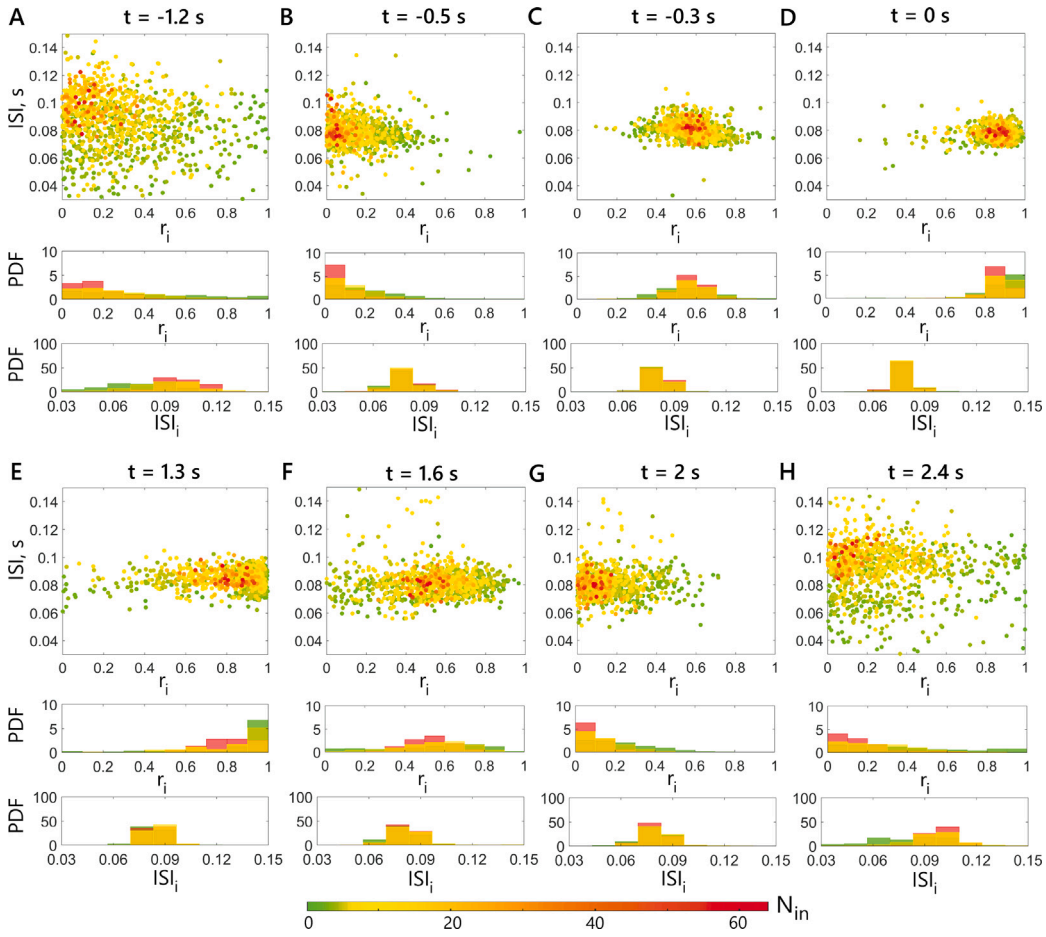

Fig. A.9. The emergence and suppression of an extreme synchronization through the analysis of interspike intervals (ISI) data: (A–D) – the onset of an event in the time interval 1.2 s prior to the peak of the order parameter S, (E–H) – the breakdown of synchrony. Each point on these diagrams represents a specific neuron, and its color corresponds to N_{in}, the total number of incoming connections. Beneath each diagram are the corresponding ISI and the r_i index distributions. PDF is probability density function. During the initiation of synchrony, ISIs coalesce into a narrow band of values, after that one can see the alignment of spiking phases and the progression of individual r_i indices towards 1. Conversely, during the suppression of the synchronous mode, this process reverses. Notably, the ISI behavior of neurons with different connectivity levels does not exhibit statistically significant differences.

the extracellular space, a consequence of glial activity [45]. The remarkable synchronicity of neurons during the ictal period is facilitated by astrocyte communication through gap junctions. Conversely, the preictal state is characterized by the presence of only locally synchronized groups of neurons. Notably, glial networks have been observed to activate and synchronize over long distances, independent of neuronal activity and synchronicity, suggesting that synaptic transmission extends beyond neuronal ensembles during epileptiform activity [45]. Integrating these findings into multiplexed epilepsy models will allow for a more comprehensive representation of the triggering mechanisms underlying the emergence and suppression of extreme synchronization events in epileptiform activity.

Future work will also be focused on investigating the balance between excitation and inhibition in the network; exploring diverse network architectures, such as small-world and random networks; testing scenarios for the occurrence and suppression of extreme synchronous events; identifying biophysical characteristics that determine the pathology of different epileptic types; and ultimately, discovering dynamic correlates that predict the transition from a preictal state to a generalized seizure.

Dynamic modeling of nonlinear processes in neurophysiology holds immense promise for unraveling the complexities of brain function, especially in the context of epilepsy. Through the application of these powerful tools, researchers can gain a deeper understanding of the intricate interactions between neurons, astrocytes, and other cell types. This knowledge can ultimately contribute to the development of more effective diagnostic and therapeutic strategies for this debilitating neurological disorder.

CRediT authorship contribution statement

Yuliya Tsybina: Writing – review & editing, Writing – original draft, Visualization, Software, Methodology, Investigation, Formal analysis, Data curation, Conceptualization. **Innokentiy Kastalskiy:** Writing – review & editing, Writing – original draft, Software, Investigation, Formal analysis, Conceptualization. **Victor B. Kazantsev:** Writing – review & editing, Writing – original draft, Supervision, Methodology, Funding acquisition, Conceptualization. **Alexander E. Hramov:** Writing – review & editing, Writing – original draft, Validation, Investigation, Conceptualization. **Susanna Gordleeva:** Writing – review & editing, Writing – original draft, Visualization, Validation, Supervision, Project administration, Methodology, Investigation, Funding acquisition, Formal analysis, Conceptualization.

Ethical statement

This article does not contain any studies involving animals performed by any of the authors.

This article does not contain any studies involving human participants performed by any of the authors.

Code availability

The code is available at https://github.com/altergot/Extreme-Synchronization-in-a-Neuron-Astrocyte-Network-A-Model-of-Epileptic-Seizures.

Declaration of competing interest

The authors declare that they have no known competing financial interests or personal relationships that could have appeared to influence the work reported in this paper.

Acknowledgment

This work was supported by the Russian Science Foundation, Russia in part by the project No. 25-69-00047 (comparison of simulation and experimental results) and in part by the project No. 23-71-30010 (conceptual work on designing a spiking neural-astrocyte network model and numerical simulations).

Appendix. Simplified neuron-astrocyte network model

In this Appendix, we present key results obtained from simulations of a simplified neuron-astrocyte network model. We examine the limiting case of complete absence of inhibition in the network, coupled with reduced astrocytic coverage where each astrocyte is individually associated with a single neuron. The model configuration consists of $N = 1000$ excitatory neurons and an equal number of astrocytes ($A = 1000$). The model contains the following changes in the description of the mechanisms of neuron-astrocytic interaction: $imp_{\text{glu}} = 500$, $G_{\text{thr}} = 0.022$;

$$J_{\text{glu}} = \begin{cases} imp_{\text{glu}} G, & \text{if} \quad G > G_{\text{thr}}, \\ 0, & \text{otherwise.} \end{cases} \tag{A.1}$$

The simplified model demonstrates a self-organized bistable regime characterized by transient extreme synchronization events in slightly different ranges of model parameters compared to the full model presented in the main text. As evidenced in Figs. A.7–A.9, the system demonstrates a more pronounced extreme synchronization effect. This manifests as transition to synchronous states with both higher neuronal synchronization levels and consequently elevated global order parameter values. Due to the lack of inhibitory neurons, epileptiform activity exhibits tighter spike synchronization, achieving near-maximal global order parameter values ($S \approx 1$) compared to the full network model ($S \approx 0.9$). Similarly, astrocytes coupled to single neurons display heightened calcium activity correlation.

References

[1] R.S. Fisher, W.v.E. Boas, W. Blume, C. Elger, P. Genton, P. Lee, J. Engel, Epileptic seizures and epilepsy: Definitions proposed by the international league against epilepsy (ILAE) and the international bureau for epilepsy (IBE), Epilepsia 46 (4) (2005) 470–472, http://dx.doi.org/10.1111/j.0013-9580.2005.66104.x.

[2] P. Kwan, S.C. Schachter, M.J. Brodie, Drug-resistant epilepsy, N. Engl. J. Med. 365 (10) (2011) 919–926, http://dx.doi.org/10.1056/nejmra1004418.

[3] J. de Tisi, G.S. Bell, J.L. Peacock, A.W. McEvoy, W.F. Harkness, J.W. Sander, J.S. Duncan, The long-term outcome of adult epilepsy surgery, patterns of seizure remission, and relapse: a cohort study, Lancet 378 (9800) (2011) 1388–1395, http://dx.doi.org/10.1016/s0140-6736(11)60890-8.

[4] P. Perucca, F.G. Gilliam, Adverse effects of antiepileptic drugs, Lancet Neurol. 11 (9) (2012) 792–802, http://dx.doi.org/10.1016/s1474-4422(12)70153-9.

[5] E. van Diessen, S.J.H. Diederen, K.P.J. Braun, F.E. Jansen, C.J. Stam, Functional and structural brain networks in epilepsy: What have we learned? Epilepsia 54 (11) (2013) 1855–1865, http://dx.doi.org/10.1111/epi.12350.

[6] J.T. Paz, J.R. Huguenard, Microcircuits and their interactions in epilepsy: Is the focus out of focus? Nature Neurosci. 18 (3) (2015) 351–359, http://dx.doi.org/10.1038/nn.3950.

[7] C.A. Schevon, S.A. Weiss, G. McKhann, R.R. Goodman, R. Yuste, R.G. Emerson, A.J. Trevelyan, Evidence of an inhibitory restraint of seizure activity in humans, Nat. Commun. 3 (1) (2012) http://dx.doi.org/10.1038/ncomms2056.

[8] N. de Lanerolle, J. Kim, R. Robbins, D. Spencer, Hippocampal interneuron loss and plasticity in human temporal lobe epilepsy, Brain Res. 495 (2) (1989) 387–395, http://dx.doi.org/10.1016/0006-8993(89)90234-5.

[9] D.C. Patel, B.P. Tewari, L. Chaunsali, H. Sontheimer, Neuron–glia interactions in the pathophysiology of epilepsy, Nature Rev. Neurosci. 20 (5) (2019) 282–297, http://dx.doi.org/10.1038/s41583-019-0126-4.

[10] M.A. Kramer, S.S. Cash, Epilepsy as a disorder of cortical network organization, Neurosci. 18 (4) (2012) 360–372, http://dx.doi.org/10.1177/1073858411422754.

[11] B.S. Chang, D.H. Lowenstein, Epilepsy, N. Engl. J. Med. 349 (13) (2003) 1257–1266, http://dx.doi.org/10.1056/nejmra022308.

[12] K. Heuser, R. Enger, Astrocytic Ca2+ signaling in epilepsy, Front. Cell. Neurosci. 15 (2021) http://dx.doi.org/10.3389/fncel.2021.695380.

[13] A. Vezzani, T. Ravizza, P. Bedner, E. Aronica, C. Steinhäuser, D. Boison, Astrocytes in the initiation and progression of epilepsy, Nat. Rev. Neurol. 18 (12) (2022) 707–722, http://dx.doi.org/10.1038/s41582-022-00727-5.

[14] S. Robel, H. Sontheimer, Glia as drivers of abnormal neuronal activity, Nature Neurosci. 19 (1) (2015) 28–33, http://dx.doi.org/10.1038/nn.4184.

[15] O. Devinsky, A. Vezzani, S. Najjar, N.C. De Lanerolle, M.A. Rogawski, Glia and epilepsy: Excitability and inflammation, Trends Neurosci. 36 (3) (2013) 174–184, http://dx.doi.org/10.1016/j.tins.2012.11.008.

[16] B.S. Khakh, M.V. Sofroniew, Diversity of astrocyte functions and phenotypes in neural circuits, Nature Neurosci. 18 (7) (2015) 942–952, http://dx.doi.org/10.1038/nn.4043.

[17] J. Zhao, J. Sun, Y. Zheng, Y. Zheng, Y. Shao, Y. Li, F. Fei, C. Xu, X. Liu, S. Wang, Y. Ruan, J. Liu, S. Duan, Z. Chen, Y. Wang, Activated astrocytes attenuate neocortical seizures in rodent models through driving Na^+-K^+-ATPase, Nat. Commun. 13 (1) (2022) http://dx.doi.org/10.1038/s41467-022-34662-2.

[18] A. Verkhratsky, A. Butt, B. Li, P. Illes, R. Zorec, A. Semyanov, Y. Tang, M.V. Sofroniew, Astrocytes in human central nervous system diseases: A frontier for new therapies, Signal Transduct. Target. Ther. 8 (1) (2023) http://dx.doi.org/10.1038/s41392-023-01628-9.

[19] N. Bazargani, D. Attwell, Astrocyte calcium signaling: The third wave, Nature Neurosci. 19 (2) (2016) 182–189, http://dx.doi.org/10.1038/nn.4201.

[20] M. Santello, N. Toni, A. Volterra, Astrocyte function from information processing to cognition and cognitive impairment, Nature Neurosci. 22 (2) (2019) 154–166, http://dx.doi.org/10.1038/s41593-018-0325-8.

[21] I. Savtchouk, A. Volterra, Gliotransmission: Beyond black-and-white, J. Neurosci. 38 (1) (2018) 14–25, http://dx.doi.org/10.1523/jneurosci.0017-17.2017.

[22] C.A. Durkee, A. Araque, Diversity and specificity of astrocyte–neuron communication, Neuroscience 396 (2019) 73–78, http://dx.doi.org/10.1016/j.neuroscience.2018.11.010.

[23] A. Araque, G. Carmignoto, P.G. Haydon, S.H. Oliet, R. Robitaille, A. Volterra, Gliotransmitters travel in time and space, Neuron 81 (4) (2014) 728–739, http://dx.doi.org/10.1016/j.neuron.2014.02.007.

[24] A. Semyanov, C. Henneberger, A. Agarwal, Making sense of astrocytic calcium signals — from acquisition to interpretation, Nature Rev. Neurosci. 21 (10) (2020) 551–564, http://dx.doi.org/10.1038/s41583-020-0361-8.

[25] N. Frolov, A. Hramov, Extreme synchronization events in a kuramoto model: The interplay between resource constraints and explosive transitions, Chaos: Interdiscip. J. Nonlinear Sci. 31 (6) (2021) http://dx.doi.org/10.1063/5.0055156.

[26] N. Frolov, A. Hramov, Self-organized bistability on scale-free networks, Phys. Rev. E 106 (4) (2022) http://dx.doi.org/10.1103/physreve.106.044301.

[27] Q. Ji, X. Qie, M. Ye, Dynamical analysis of astrocyte-induced neuronal hyperexcitation, Nonlinear Dynam. 111 (8) (2022) 7713–7728, http://dx.doi.org/10.1007/s11071-022-08202-y.

[28] J. Li, R. Wang, M. Du, J. Tang, Y. Wu, Dynamic transition on the seizure-like neuronal activity by astrocytic calcium channel block, Chaos Solitons Fractals 91 (2016) 702–708, http://dx.doi.org/10.1016/j.chaos.2016.08.009.

[29] J. Li, J. Tang, J. Ma, M. Du, R. Wang, Y. Wu, Dynamic transition of neuronal firing induced by abnormal astrocytic glutamate oscillation, Sci. Rep. 6 (1) (2016) http://dx.doi.org/10.1038/srep32343.

[30] M. Du, J. Li, L. Chen, Y. Yu, Y. Wu, Astrocytic kir4.1 channels and gap junctions account for spontaneous epileptic seizure, in: W.W. Lytton (Ed.), PLoS Comput. Biol. 14 (3) (2018) e1005877, http://dx.doi.org/10.1371/journal.pcbi.1005877.

[31] Y. Wei, G. Ullah, J. Ingram, S.J. Schiff, Oxygen and seizure dynamics: II. Computational modeling, J. Neurophysiol. 112 (2) (2014) 213–223, http://dx.doi.org/10.1152/jn.00541.2013.

[32] D.A. McCormick, D. Contreras, On the cellular and network bases of epileptic seizures, Annu. Rev. Physiol. 63 (1) (2001) 815–846, http://dx.doi.org/10.1146/annurev.physiol.63.1.815.

[33] P. Bedner, A. Dupper, K. Hüttmann, J. Müller, M.K. Herde, P. Dublin, T. Deshpande, J. Schramm, U. Häussler, C.A. Haas, C. Henneberger, M. Theis, C. Steinhäuser, Astrocyte uncoupling as a cause of human temporal lobe epilepsy, Brain 138 (5) (2015) 1208–1222, http://dx.doi.org/10.1093/brain/awv067.

[34] J. Zhao, Y. Yu, F. Han, Q. Wang, Dynamic modeling and closed-loop modulation for absence seizures caused by abnormal glutamate uptake from astrocytes, Nonlinear Dynam. 112 (5) (2024) 3903–3916, http://dx.doi.org/10.1007/s11071-023-09218-8.

[35] J. Zhao, Y. Yu, Q. Wang, Dynamical regulation of epileptiform discharges caused by abnormal astrocyte function with optogenetic stimulation, Chaos Solitons Fractals 164 (2022) 112720, http://dx.doi.org/10.1016/j.chaos.2022.112720.

[36] J. Li, J. Song, N. Tan, C. Cao, M. Du, S. Xu, Y. Wu, Channel block of the astrocyte network connections accounting for the dynamical transition of epileptic seizures, Nonlinear Dynam. 105 (4) (2021) 3571–3583, http://dx.doi.org/10.1007/s11071-021-06737-0.

[37] J. Tang, J. Zhang, J. Ma, G. Zhang, X. Yang, Astrocyte calcium wave induces seizure-like behavior in neuron network, Sci. China Technol. Sci. 60 (7) (2016) 1011–1018, http://dx.doi.org/10.1007/s11431-016-0293-9.

[38] G. Ullah, J.R. Cressman Jr., E. Barreto, S.J. Schiff, The influence of sodium and potassium dynamics on excitability, seizures, and the stability of persistent states: II. Network and glial dynamics, J. Comput. Neurosci. 26 (2) (2008) 171–183, http://dx.doi.org/10.1007/s10827-008-0130-6.

[39] M. Amiri, F. Bahrami, M. Janahmadi, On the role of astrocytes in epilepsy: A functional modeling approach, Neurosci. Res. 72 (2) (2012) 172–180, http://dx.doi.org/10.1016/j.neures.2011.11.006.

[40] V. Grigorovsky, V.L. Breton, B.L. Bardakjian, Glial modulation of electrical rhythms in a neuroglial network model of epilepsy, IEEE Trans. Biomed. Eng. 68 (7) (2021) 2076–2087, http://dx.doi.org/10.1109/tbme.2020.3022332.

[41] Y. Yu, Z. Yuan, Y. Fan, J. Li, Y. Wu, Dynamic transitions in neuronal network firing sustained by abnormal astrocyte feedback, in: R. Wang (Ed.), Neural Plast. 2020 (2020) 1–13, http://dx.doi.org/10.1155/2020/8864246.

[42] I. Pavlov, M.C. Walker, Tonic $GABA_A$ receptor-mediated signalling in temporal lobe epilepsy, Neuropharmacology 69 (2013) 55–61, http://dx.doi.org/10.1016/j.neuropharm.2012.04.003.

[43] S. Pandit, C. Neupane, J. Woo, R. Sharma, M.-H. Nam, G.-S. Lee, M.-H. Yi, N. Shin, D.W. Kim, H. Cho, B.H. Jeon, H.-W. Kim, C.J. Lee, J.B. Park, Bestrophin1-mediated tonic GABA release from reactive astrocytes prevents the development of seizure-prone network in kainate-injected hippocampi, Glia 68 (5) (2019) 1065–1080, http://dx.doi.org/10.1002/glia.23762.

[44] J. Müller, A. Timmermann, L. Henning, H. Müller, C. Steinhäuser, P. Bedner, Astrocytic GABA accumulation in experimental temporal lobe epilepsy, Front. Neurol. 11 (2020) http://dx.doi.org/10.3389/fneur.2020.614923.

[45] C. Diaz Verdugo, S. Myren-Svelstad, E. Aydin, E. Van Hoeymissen, C. Deneubourg, S. Vanderhaeghe, J. Vancraeynest, R. Pelgrims, M.I. Cosacak, A. Muto, C. Kizil, K. Kawakami, N. Jurisch-Yaksi, E. Yaksi, Glia-neuron interactions underlie state transitions to generalized seizures, Nat. Commun. 10 (1) (2019) http://dx.doi.org/10.1038/s41467-019-11739-z.

[46] J.T. Paz, T.J. Davidson, E.S. Frechette, B. Delord, I. Parada, K. Peng, K. Deisseroth, J.R. Huguenard, Closed-loop optogenetic control of thalamus as a tool for interrupting seizures after cortical injury, Nature Neurosci. 16 (1) (2012) 64–70, http://dx.doi.org/10.1038/nn.3269.

[47] C.L. Yasuda, Z. Chen, G.C. Beltramini, A.C. Coan, M.E. Morita, B. Kubota, F. Bergo, C. Beaulieu, F. Cendes, D.W. Gross, Aberrant topological patterns of brain structural network in temporal lobe epilepsy, Epilepsia 56 (12) (2015) 1992–2002, http://dx.doi.org/10.1111/epi.13225.

[48] D. Fan, H. Wu, G. Luan, Q. Wang, The potential scale-free network mechanism underlying the formation of focal epilepsy, Europhys. Lett. 141 (3) (2023) 32002, http://dx.doi.org/10.1209/0295-5075/acb381.

[49] X. Liu, Y. Yu, Q. Wang, Dynamic epileptic seizure propagation based on multiscale synaptic plasticity, Nonlinear Dynam. (2024) http://dx.doi.org/10.1007/s11071-024-10590-2.

[50] E. Izhikevich, Simple model of spiking neurons, IEEE Trans. Neural Networks 14 (6) (2003) 1569–1572, http://dx.doi.org/10.1109/tnn.2003.820440.

[51] A.-L. Barabasi, R. Albert, Emergence of scaling in random networks, Science 286 (5439) (1999) 509–512, http://dx.doi.org/10.1126/science.286.5439.509.

[52] V.B. Kazantsev, S.Y. Asatryan, Bistability induces episodic spike communication by inhibitory neurons in neuronal networks, Phys. Rev. E 84 (3) (2011) http://dx.doi.org/10.1103/physreve.84.031913.

[53] P.M. Esir, S.Y. Gordleeva, A.Y. Simonov, A.N. Pisarchik, V.B. Kazantsev, Conduction delays can enhance formation of up and down states in spiking neuronal networks, Phys. Rev. E 98 (5) (2018) http://dx.doi.org/10.1103/physreve.98.052401.

[54] G. Ullah, P. Jung, A. Cornell-Bell, Anti-phase calcium oscillations in astrocytes via inositol (1, 4, 5)-trisphosphate regeneration, Cell Calcium 39 (3) (2006) 197–208, http://dx.doi.org/10.1016/j.ceca.2005.10.009.

[55] T. Yamamoto, A. Ochalski, E.L. Hertzberg, J.I. Nagy, On the organization of astrocytic gap junctions in rat brain as suggested by LM and EM immunohistochemistry of connexin43 expression, J. Comp. Neurol. 302 (4) (1990) 853–883, http://dx.doi.org/10.1002/cne.903020414.

[56] J.I. Nagy, J.E. Rash, Connexins and gap junctions of astrocytes and oligodendrocytes in the CNS, Brain Res. Rev. 32 (1) (2000) 29–44, http://dx.doi.org/10.1016/s0165-0173(99)00066-1.

[57] S.Y. Gordleeva, S.V. Stasenko, A.V. Semyanov, A.E. Dityatev, V.B. Kazantsev, Bi-directional astrocytic regulation of neuronal activity within a network, Front. Comput. Neurosci. 6 (2012) http://dx.doi.org/10.3389/fncom.2012.00092.

[58] E.V. Pankratova, A.I. Kalyakulina, S.V. Stasenko, S.Y. Gordleeva, I.A. Lazarevich, V.B. Kazantsev, Neuronal synchronization enhanced by neuron–astrocyte interaction, Nonlinear Dynam. 97 (1) (2019) 647–662, http://dx.doi.org/10.1007/s11071-019-05004-7.

[59] S. Lee, B.-E. Yoon, K. Berglund, S.-J. Oh, H. Park, H.-S. Shin, G.J. Augustine, C.J. Lee, Channel-mediated tonic GABA release from glia, Science 330 (6005) (2010) 790–796, http://dx.doi.org/10.1126/science.1184334.

[60] M. Khoshkhou, A. Montakhab, Beta-rhythm oscillations and synchronization transition in network models of izhikevich neurons: Effect of topology and synaptic type, Front. Comput. Neurosci. 12 (2018) http://dx.doi.org/10.3389/fncom.2018.00059.

[61] S. Boccaletti, J. Kurths, G. Osipov, D. Valladares, C. Zhou, The synchronization of chaotic systems, Phys. Rep. 366 (1–2) (2002) 1–101, http://dx.doi.org/10.1016/s0370-1573(02)00137-0.

[62] J. Gómez-Gardeñes, S. Gómez, A. Arenas, Y. Moreno, Explosive synchronization transitions in scale-free networks, Phys. Rev. Lett. 106 (12) (2011) http://dx.doi.org/10.1103/physrevlett.106.128701.

[63] H. Chen, G. He, F. Huang, C. Shen, Z. Hou, Explosive synchronization transitions in complex neural networks, Chaos: An Interdiscip. J. Nonlinear Sci. 23 (3) (2013) http://dx.doi.org/10.1063/1.4818543.

[64] B.R.R. Boaretto, R.C. Budzinski, T.L. Prado, S.R. Lopes, Mechanism for explosive synchronization of neural networks, Phys. Rev. E 100 (5) (2019) http://dx.doi.org/10.1103/physreve.100.052301.

[65] E. Sitnikova, A.E. Hramov, V.V. Grubov, A.A. Ovchinnkov, A.A. Koronovsky, On–off intermittency of thalamo-cortical oscillations in the electroencephalogram of rats with genetic predisposition to absence epilepsy, Brain Res. 1436 (2012) 147–156, http://dx.doi.org/10.1016/j.brainres.2011.12.006.

[66] A. Hramov, A.A. Koronovskii, I.S. Midzyanovskaya, E. Sitnikova, C.M. van Rijn, On-off intermittency in time series of spontaneous paroxysmal activity in rats with genetic absence epilepsy, Chaos: An Interdiscip. J. Nonlinear Sci. 16 (4) (2006) http://dx.doi.org/10.1063/1.2360505.

[67] A.A. Koronovskii, A.E. Hramov, V.V. Grubov, O.I. Moskalenko, E. Sitnikova, A.N. Pavlov, Coexistence of intermittencies in the neuronal network of the epileptic brain, Phys. Rev. E 93 (3) (2016) http://dx.doi.org/10.1103/physreve.93.032220.

[68] N.S. Frolov, V.V. Grubov, V.A. Maksimenko, A. Lüttjohann, V.V. Makarov, A.N. Pavlov, E. Sitnikova, A.N. Pisarchik, J. Kurths, A.E. Hramov, Statistical properties and predictability of extreme epileptic events, Sci. Rep. 9 (1) (2019) http://dx.doi.org/10.1038/s41598-019-43619-3.